Chem Biol Drug Des 2012; **79:** 819–834

Research Letter

doi: 10.1111/j.1747-0285.2012.01335.x

Prodrugs of Acyclovir – A Computational Approach

Rafik Karaman[1,*], Khuloud K. Dajani[2], Alaa Qtait[1] and Mustafa Khamis[3]

[1]*Faculty of Pharmacy, Al-Quds University, P. O. Box 20002, Jerusalem, Palestine*
[2]*Faculty of Public Health Sciences, Al-Quds University, P. O. Box 20002, Jerusalem, Palestine*
[3]*Department of Chemistry and Chemical Technology, Al-Quds University, P. O. Box 20002, Jerusalem, Palestine*
**Corresponding author: Rafik Karaman, dr_karaman@yahoo.com*

Density functional theory calculation results demonstrated that the efficiency of the acid-catalyzed hydrolysis of Kirby's acid amides 1–15 is strongly dependent on the substitution on the C–C double bond and the nature of the amide *N*-alkyl group. Further, the results established that while in the gas phase the hydrolysis rate-limiting step is the tetrahedral intermediate formation in polar solvents such as water, the rate-limiting step could be either the formation or the collapse of the tetrahedral intermediate depending on the substitution on the C–C double bond and on the amide nitrogen substituent. Based on a linear correlation between the calculated and experimental effective molarities, the study on the systems reported herein could provide a good basis for designing prodrug systems that are less hydrophilic than their parental drugs and can be used, in different dosage forms, to release the parent drug in a controlled manner. For example, based on the calculated log effective molarities values, the predicted $t_{1/2}$ (a time needed for 50% of the reactant to be hydrolyzed to products) for acyclovir prodrugs, ProD 1–4, was 29.2 h, 6097 days, 4.6 min, and 8.34 h, respectively. Hence, the rate by which acyclovir prodrug releases acyclovir can be determined according to the structural features of the linker (Kirby's acid amide moiety).

Key words: acyclovir prodrugs, bioavailability of acyclovir, density functional theory calculations, intramolecular amide hydrolysis, maleamic acid amides

Received 20 September 2011, revised 29 November 2011 and accepted for publication 29 December 2011

Acyclovir is a synthetic acyclic purine nucleoside analog that is the first agent to be licensed for the prevention and treatment for viral infections such as herpes simplex (HSV), varicella zoster (chicken pox), and herpes zoster (shingles) (1). Acyclovir is poorly water soluble and has an oral bioavailability of 10–20%; hence, intravenous administration is necessary if high dosing is required. When orally administered, peak plasma concentration occurs after 1–2 h. Acyclovir has a high distribution rate with only 30% is protein-bound in plasma. The elimination half-life of acyclovir is about 3 h. It is renally excreted by both glomerular filtration and tubular secretion (2).

Acyclovir is marketed as tablets of 200, 400, and 800 mg, suspension for oral administration, intravenous injection, and ophthalmic and skin topical creams. Per os acyclovir is mostly used as 200 mg tablets, five times daily. In addition, 6 month to a year administration of acyclovir is required in immunocompetent patient with relapsing herpes simplex infection (2).

The currently available oral administration therapy is associated with a number of drawbacks such as highly variable absorption and low bioavailability (10–20%). The main problem with the therapeutic effectiveness of acyclovir is its absorption that is highly variable and dose dependent, thus reducing the bioavailability to 10–20%. In commercially available dosages forms of acyclovir, the amount of drug absorbed is very low because of short residence time of the dosage forms at the absorption site. In humans, acyclovir showed poor and variable oral bioavailability (10–20%), probably due to the relatively low lipophilicity of the drug. Thus, the rate-limiting factor in acyclovir absorption is its membrane permeability (3).

Several approaches have been made to improve the oral bioavailability of acyclovir: (i) Luengo *et al.* have used different preparations of acyclovir with β-cyclodextrin in order to increase its solubility and hence its bioavailability; however, no significant effect of β-cyclodextrin on the oral drug bioavailability was observed. This was attributed to the effect of β-cyclodextrin only on the solubility and not on the permeability of the drug (4). (ii) Encapsulation of acyclovir in lipophilic vesicular structure was carried out to enhance the oral absorption and prolong the existence of the drug in the systemic circulation. This was accomplished by niosomes (non-ionic surfactant vesicles) that are well recognized as drug delivery vehicles. *In vivo* study by El-Gizawy and coworkers using niosomal formulation revealed that the niosomal dispersion significantly improved the oral bioavailability of acyclovir in rabbits after a single oral dose of 40 mg/kg. The average relative bioavailability of the drug from the niosomal dispersion in relation to the free solution indicated more than twofold increase in drug bioavailability. The niosomal dispersion showed significant increase in the mean residence time of acyclovir reflecting sustained release characteristics (5). (iii) Yadav *et al.* have used acyclovir-loaded mucoadhesive

microspheres for increasing the retention time and hence the bioavailability of acyclovir. Their study revealed that the microspheres prepared from sodium CMC having high mucoadhesiveness and fair entrapment efficiency enabled the sustained release of acyclovir from microspheres and plasma drug concentration in rabbits was maintained for 24 h (6), and (iv) the search for an effective prodrug that would provide acyclovir with higher bioavailability led to the synthesis of a number of aliphatic and amino acid esters of acyclovir. Among these compounds was the L-valyl ester, valacyclovir HCl (Scheme 1). Valacyclovir has greater oral bioavailability (about 55%) than acyclovir (10–20%). It is converted by esterases to the active drug acyclovir, as well as the amino acid valine, via hepatic first-pass metabolism (7). Another prodrugs approach for enhancing acyclovir oral bioavailability was by utilizing the human apical sodium-dependent bile acid transporter (hASBT). Using each chenodeoxycholate, deoxycholate, cholate, and ursodeoxycholate, four bile acid prodrugs of acyclovir were synthesized, where acyclovir was conjugated to a bile acid via a valine linker. Relative to cellular uptake studies of acyclovir alone, the cellular uptake from the prodrug resulted in a 16-fold greater acyclovir accumulation within hASBT-COS cells, indicating enhanced permeation properties of the prodrug. Enhanced permeability was attributable to hASBT-mediated uptake and increased passive permeability. Furthermore, it was found that oral administration of acyclovir valylchenodeoxycholate to rats resulted in a twofold increase in the bioavailability of acyclovir, compared with the bioavailability after the administration of acyclovir alone (8).

After reviewing the literature on the physical properties and pharmacokinetics of acyclovir, it is quite safe to assume that its low bioavailability is attributable mainly to inefficient permeability through membranes rather than its insolubility in physiologic environments, especially in acidic medium such as stomach. Hence, improvement of acyclovir pharmacokinetic properties and hence their effectiveness may increase the absorption of acyclovir via a variety of administration routes. This can be achieved by utilizing a carrier-linked prodrug strategy which could be done by linking acyclovir to a carrier moiety to furnish a drug-host system which upon exposure to physiological environment, such as stomach or intestine, can penetrate the membrane tissues and liberate the active drug, acyclovir, in a controlled manner.

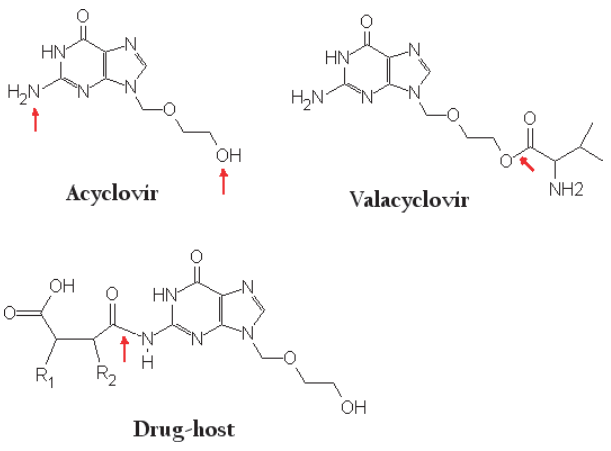

Scheme 1: Chemical structures for acyclovir, valacyclovir, and drug-host.

The approach of covalently linking a valyl moiety to acyclovir free hydroxyl group to give the ester derivative of acyclovir (valacyclovir) had succeeded to increase the antiviral drug bioavailability approximately threefold (from 20% to 55%) (7). However, further improvement of the structural features of acyclovir is still to be made in order to obtain a prodrug that might have a higher bioavailability than the current prodrug (valacyclovir). It should be noted that valacyclovir prodrug might suffer from partial hydrolysis by esterases upon reaching the stomach that results in a decrease in its bioavailability.

For achieving acyclovir prodrug with higher bioavailability, the prodrug must be characterized with the following properties: (i) to be readily soluble in a physiological medium, (ii) to have a moderate hydrophilic–lipophilic balance (HLB) value such that allowing an efficient permeability, (iii) to release the active drug in a controlled manner once it reaches the target, and (iv) to yield upon cleavage a safe and non-toxic by-products. By making a prodrug with these physical and chemical properties, the following goals might be accomplished: (i) a relatively high permeability of the prodrug through the tissues, (ii) a higher feasibility for using the drug in different dosage forms, (iii) a chemically driven system that liberates acyclovir in a controlled manner upon reaching the human blood circulation system, and (iv) an antiviral drug with physical–chemical properties such that leading to a high bioavailability and efficient pharmacokinetic properties.

A large number of prodrugs have been designed and developed in order to improve the effectiveness of certain drugs and to overcome pharmaceutical and pharmacokinetic barriers upon drug administration, such as low absorption, chemical instability, low solubility, and poor patient compliance. For example, valacyclovir prodrug was designed and synthesized in order to overcome low permeability of acyclovir. Valacyclovir design was based on biochemical approach by which the prodrug will be hydrolyzed to acyclovir by esterase enzymes once it penetrates the membrane tissues (7).

Recently, we have been investigating the mechanisms for some intramolecular processes that have been utilized to understand enzyme catalysis and lately have been exploited as prodrug linkers (9–17). Using density functional theory (DFT) and *ab initio* molecular orbital methods, we have studied various intramolecular processes among them: (i) proton transfer between two oxygens in Kirby's acetals (11), and proton transfer between nitrogen and oxygen in Kirby's enzyme models (15,18–27), (ii) proton transfer between two oxygens in rigid systems as investigated by Menger (9,28–35), and (iii) proton transfer from oxygen to carbon in some of Kirby's enol ethers (16,18–27) arriving at the following conclusions: (i) rate enhancement in intramolecular processes is a result of both entropy and enthalpy effects. In intramolecular cyclization processes where enthalpic effects were predominant, steric effects was the driving force for the accelerations, whereas proximity orientation was the determining factor in the cases of proton-transfer reactions. (ii) The distance between the two reacting centers is the main factor to determine whether the reaction type is intermolecular or intramolecular. In the cases by which the distance exceeded 3 Å, an intermolecular

engagement was preferred because of the involvement of a water molecule (solvent), whereas an intramolecular engagement prevailed when the distance between the electrophile and nucleophile was <3 Å. (iii) The efficiency of proton transfer between two oxygens and between nitrogen and oxygen in Kirby's enzyme models is attributed to a relatively strong hydrogen bonding developed in the products and the transition states leading to them.

We have learned from our recent studies on intramolecularity that there is a crucial necessity to investigate the reaction mechanism for assigning the factors determining the reaction rate for a better design of an efficient chemical device to be exploited as prodrug linker and to have the potential to chemically (not via enzymes) liberate the active drug in a programmable (controlled) manner. For example, we have explored the mechanism for the proton transfer in Kirby's acetals (18–27), and based on our findings, we have designed prodrugs of aza nucleosides for the treatment of myelodysplastic syndromes where the prodrug linker is attached to the hydroxyl group of the nucleoside (15). In addition, prodrugs of paracetamol capable of masking the bitter taste of the parental drug, paracetamol, were also designed such that the linker is covalently linked to the phenolic group of paracetamol which is believed to be responsible for the bitterness of the drug (17). The prodrugs were designed such that they will undergo cleavage reactions in physiological environments such as stomach at pH 1.5, intestine at pH 6.5, and/or blood circulation at pH 7.4, with rates that are solely dependent on the structural features of the pharmacologically inactive linker. Different linkers were also investigated for the design of large number of prodrugs, such as anti-Parkinson, antimalarial, and antihypertensive, that might be efficient in releasing the parental drugs in various rates that are dependent on the nature or the structural features of the linkers (13).

To expand our approach for utilizing intramolecularity to design potential linkers for amine drugs, we have studied the mechanism and driving forces determining the rate of the acid-catalyzed hydrolysis in some of Kirby's acid amides (prodrugs linkers) (36,37). This work was carried out with the hope that such linkers might have a potential to be good carriers to the antiviral agent, acyclovir.

Based on the DFT calculation results on the acid-catalyzed hydrolysis of amide acids **1**–**15** reported herein (Scheme 2), four acyclovir prodrugs are proposed (Scheme 3). As shown in Scheme 3, the acyclovir prodrugs, **ProD 1**–**ProD 4** are composed of the amide acid linker having a carboxylic acid group (hydrophilic moiety) and the rest of the prodrug molecule (a lipophilic moiety). The combination of both groups secures a prodrug moiety having a potential to be with a high permeability (a moderate HLB). It should be emphasized that the HLB value of the prodrug moiety will be dependent on the pH of the target physiologic environment. In the stomach, it is expected that prodrugs **ProD 1**–**4** will be in the carboxylic acid form (a relatively high lipophilicity), whereas in the blood circulation system the carboxylate anion form (a relatively low lipophilicity) will be predominant. The plan is to prepare **ProD 1–4** (Scheme 3) as sodium or potassium carboxylate salts owing to their stability in neutral aqueous medium. It should be noted that acid amides such as **1**–**15** undergo hydrolysis in acidic aqueous medium, whereas they are relatively stable at pH 7.4.

In this article, we report a DFT computational study on intramolecular acid-catalyzed hydrolysis of 15 maleamic (4-amino-4-oxo-2butenoic) acids, **1**–**15** (Scheme 2). Based on the calculated and experimental rates for processes **1**–**15**, the $t_{1/2}$ values (the time needed for 50% of the prodrug to be hydrolyzed to the antiviral drug, acyclovir) for **ProD 1**–**4** were evaluated.

The aims of this work were to (i) study the mechanistic behavior of the acid-catalyzed hydrolysis for several maleamic acid amides having different alkyl groups on the amide nitrogen and different substitution on the carbon–carbon double bond and unravel the nature

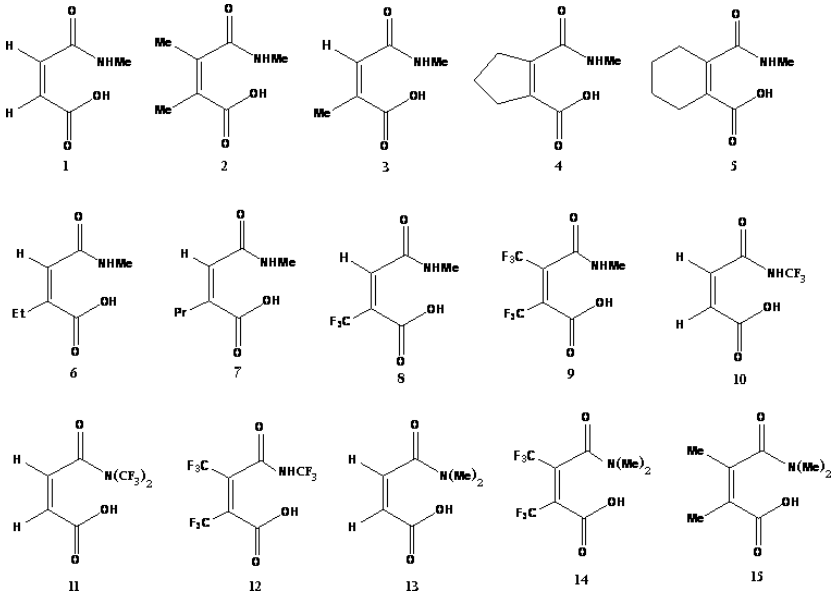

Scheme 2: Chemical structures for **1**–**15**.

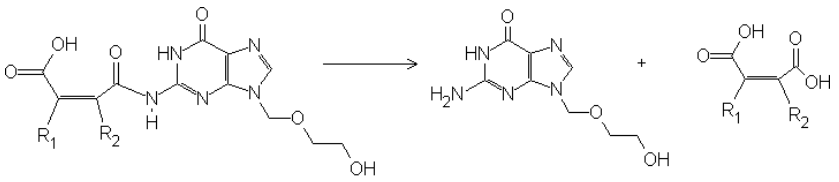

ProD 1; $R_1 = R_2 = Me$

ProD 2; $R_1 = R_2 = CF_3$

ProD 3; $R_1 = Me, R_2 = H$

ProD 4; $R_1 = R_2 = H$

Scheme 3: Chemical structures for **ProD 1**–**4**.

of the force(s) affecting the rate as a function of these substitutions, and (ii) design of various acyclovir prodrugs that are relatively tissue permeable and have the capability to undergo chemical hydrolysis (not enzymatic) in physiological environment to provide acyclovir in a sustained release manner.

Calculations Methods

The Becke three-parameter, hybrid functional combined with the Lee, Yang, and Parr correlation functional, denoted B3LYP, was employed in the calculations using DFT. All calculations were made using the quantum chemical package Gaussian-98[a]. Calculations were made based on the restricted Hartree–Fock method[a]. The starting geometries of all calculated molecules **1**–**15**, **Inter**, and **ProD 1**–**4** were obtained using the Argus Lab program (38) and were initially optimized at the HF/6-31G level of theory in the presence of one molecule of water, followed by optimization at the B3LYP/6-31G(d,p). Systems **1**–**3** were also calculated at B3LYP/311 + G (d,p) level and at the density functional from Truhlar group (hybrid GGA: MPW1k) (39). Total geometry optimizations included all internal rotations. Second derivatives were estimated for all 3N-6 geometrical parameters during optimization. The search for the global minimum structure (GM) in each of the systems studied was accomplished by 360° rotation of the carboxylic group about the bond C6–C7 (i.e., variation in the dihedral angle O1/C7/C6/C5, Chart 1) and by 360° rotation of the carbonyl amide group about the C4–C5 bond (i.e., variation in the dihedral angle O3/C4/C5/C6) in increments of 10° and calculation of the conformational energies (see Chart 1). In the DFT calculations for **1**–**15** and **ProD 1**–**4**, two types of conformations in particular were considered: one in which the amide carbonyl is *syn* to the carboxyl group and another in which it is *anti*. An energy minimum (a stable compound or a reactive intermediate) has no negative vibrational force constant. A transition state is a saddle point that has only one negative vibrational force constant (40). Transition states were located first by the normal reaction co-ordinate method (41) where the enthalpy changes were monitored by stepwise changing the interatomic distance between two specific atoms. The geometry at the highest point on the energy profile was re-optimized by using the energy gradient method at the B3LYP/6-31G(d,p) level of theory[a]. The 'reaction co-ordinate method' (41) was used to calculate the activation energy in maleamic (4-amino-4-oxo-2butenoic) acids,

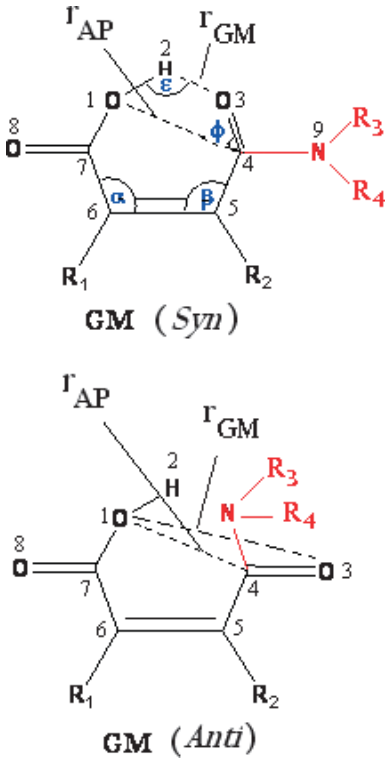

Chart 1: Chemical representation of the *syn* and *anti* conformations for the global minimum structures (GM).

1–**15**, and **ProD 1**–**4** (Schemes 2 and 3). In this method, one bond length is constrained for the appropriate degree of freedom, while all other variables are freely optimized. The activation energy values for the approach processes (the approach of O1 toward C4, Chart 1) were calculated from the difference in energies of the GM and the derived transition states (TS_2 in Scheme 4). Similarly, the activation energies of the dissociation processes (the breakdown of C4–N9 bond, Chart 1) were calculated from the difference in energies of the GM and the corresponding transition states (TS_3 in Scheme 4). Verification of the desired reactants and products was accomplished using the 'intrinsic co-ordinate method' (41). The transition-state structures were verified by their only one negative frequency. Full optimization of the transition states was accomplished after removing any constrains imposed while executing the energy

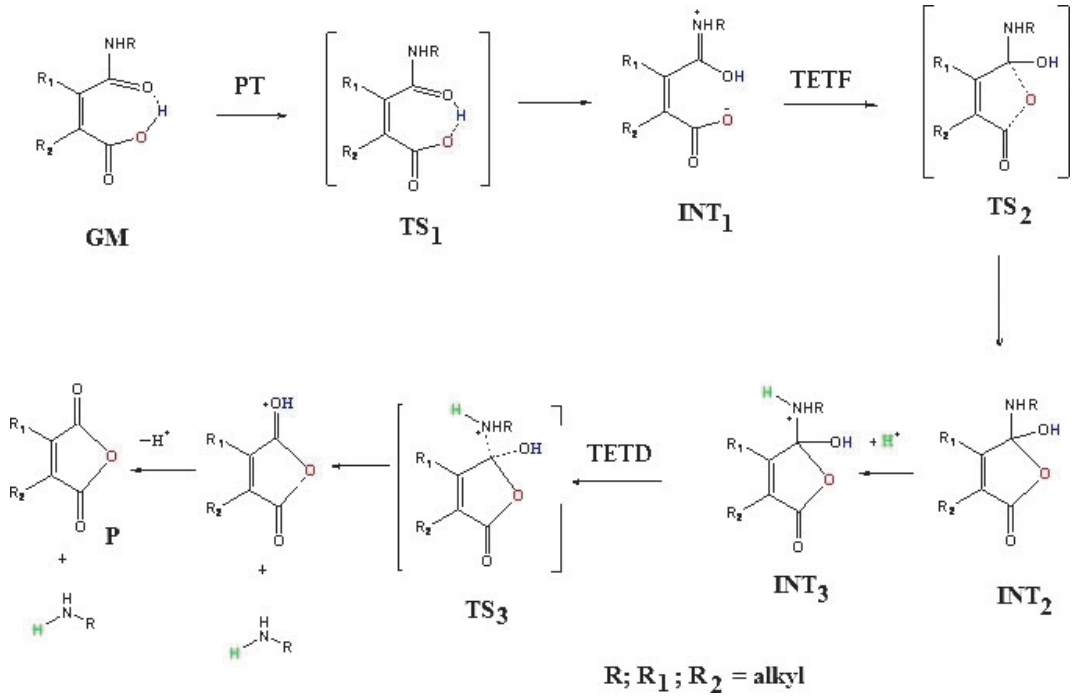

Scheme 4: Proposed mechanism for processes **1**–**15**. PT refers to proton transfer. TETF and TETD refer to tetrahedral intermediate formation and dissociation, respectively. GM, TS, INT, and P are global minimum, transition-state, intermediate and product structures, respectively.

profile. The activation energies obtained from the DFT at B3LYP/6-31G (d,p) level of theory for **1–15**, **ProD 1**–**4**, and **Inter** were calculated with and without the inclusion of solvent (water and ether). The calculations with the incorporation of a solvent were made using the integral equation formalism model of the polarizable continuum model (42–45). In this model, the cavity is created via a series of overlapping spheres. The radii type employed was the United Atom Topological Model on radii optimized for the PBE0/6-31G (d) level of theory.

Results and Discussion

In 1968, Dixon and Perham observed that the half amide formed by the reaction of arginine with dimethylmaleic anhydride is hydrolyzed more rapidly than that of the unsubstituted maleic acid derivatives (46). This observation had led Kirby and coworkers to investigate those structural factors associated with high reactivity in the intramolecular acid-catalyzed hydrolysis of nine maleamic (4-amino-4-oxo-2butenoic) acids (36,37). They found that the efficiency of the intramolecular hydrolysis is remarkably sensitive to the pattern of substitution on the carbon–carbon double bond. Further, their study revealed that the rates of the hydrolysis of the nine amide acid derivatives studied range over more than 10^{10}. Furthermore, they have concluded that the amide bond cleavage is because of intramolecular nucleophilic catalysis by the adjacent carboxylic acid group, and the rate-limiting step is the one by which dissociation of the tetrahedral intermediate occurs (36). Later on, Kluger (47) had studied the intramolecular hydrolysis mechanism of eight maleamic acids derived from aliphatic amines of a wide range of basicity. His study revealed that the identity of the rate-limiting step is a function of both the basicity of the leaving group and the acidity of the solution. In 1990, Katagi has computationally studied the acid-catalyzed hydrolysis of three maleamic (4-amino-4-oxo-2butenoic) acids using the semiempirical method AM1. In contrast to that found by Kirby, Katagi's study revealed that the rate-limiting step is the formation of the tetrahedral intermediate and not its collapse (48).

As Katagi's semiempirical calculations were run in the presence of only two molecules of water which resembles somewhat the gas-phase environment, we sought to study the acid-catalyzed hydrolysis reactions of a variety of maleamic acid amide derivatives using Becke three-parameter hybrid functional combined with the Lee, Yang, and Parr correlation functional (B3LYP) methods, which are superior to semiempirical methods, and to run the calculations in the gas phase as well as in other solvents such as ether and water because of the importance of the solvent in stabilizing or destabilizing the chemical entities involved in the hydrolysis.

As shown in Scheme 2, the 15 maleamic acid amide derivatives differ in the substituents attached to the carbon–carbon double bond and/or the alkyl group attached to the amide nitrogen. Replacing the *N*-alkyl amide group in **1**–**15** (Scheme 2) with acyclovir drug, as shown for **ProD 1**–**ProD 4** in Scheme 3, is not expected to affect significantly the relative rates of these processes. Hence, computations of the kinetic and thermodynamic parameters for processes **1**–**15** will shed light on the rates for the acid-catalyzed hydrolysis of prodrugs **ProD 1**–**ProD 4** to the antiviral drug, acyclovir.

For the use of systems **1**–**15** as prodrug linkers of acyclovir as shown in Scheme 3, the reaction mechanism for the hydrolysis of

1–**15** should be unraveled. As mentioned above, only one mechanism was suggested for this reaction; however, the question which step is the rate-limiting one is still in debate. Two different rate-limiting steps were proposed: (i) a step that involves the formation of a tetrahedral intermediate (48) and (ii) a step by which the tetrahedral intermediate dissociates to provide products (Scheme 4) (36). In order to determine the rate-limiting step, DFT calculations at the B3LYP/6-31G (d,p) level were made in the gas phase as well as in ether and water.

Computational efforts were directed toward the elucidation of the transition-state and ground-state structures (reactants, intermediates, and products) for the acid-catalyzed hydrolysis of **1**–**15** (49) and **ProD 1**–**4**. Calculations for all entities were made in the presence of one and two molecules of water in the gas phase as well as in water and ether as solvents. It is expected that the stability of the ground states and transition states will be different in solvent having low dielectric constant, such as the gas phase or ether, and solvent with high dielectric constant, such as water.

General consideration

Because the energy of a carboxylic acid amide moiety is strongly dependent on its conformation which could be engaged in inter- or intramolecular hydrogen bonding, we were concerned with the identification of the most stable conformation (global minimum) for each of the maleamic acid amides **1**–**15** and **ProD 1**–**4**. This was accomplished by 36 rotations of the carboxyl group about the bond C6–C7 in increments of 10° (i.e., variation in the dihedral angle O1/C7/C6/C5, see Chart 1) and by 360° rotation of the carbonyl amide group about the bond C4–C5 (i.e., variation in the dihedral angle O3/C4/C5/C6) in increments of 10° and calculation of the conformational energies (see Chart 1).

In the DFT calculations of the starting geometries in **1**–**15** and **ProD 1**–**4**, two different types of conformations were considered: one in which the amide carbonyl is *syn* to the carboxyl group and another in which it is *anti* (Chart 1). It was found that the GM for **1**–**15** and **ProD 1**–**4** all reside in the *syn* conformation (see Figure 1A).

Optimized structures for the entities involved in the acid-catalyzed hydrolysis of maleamic acid amides 1–15 and ProD 1–4

Reactants (GM)

Because the acid-catalyzed hydrolysis of the maleamic acid amide derivatives was conducted in aqueous medium, we have calculated the geometries of all entities involved in these hydrolysis reactions in the presence of one and two water molecules and in the gas phase (without any molecule of water). This was carried out in order to account for any specific intermolecular hydrogen bonding between water and the reactant. DFT-optimized geometries along with selected bond distances and bond angles for the reactants of **1–15** and **ProD 1**–**4**, **1GM**–**15GM**, and **ProD 1GM**–**4GM,** respectively, are illustrated in Figures 1A and 2A and listed in Table 1. Careful examination of the calculated geometries in Figures 1A and 2A indicates that all the reactants exhibit conformations by which the carboxyl group is engaged intramolecularly in a hydrogen bond with the neighboring amide oxygen to form a seven-membered ring. In the geometries of **1**–**15,** the seven-membered ring is quite normal; however, the ring in the geometries of **ProD 1**–**4** is somewhat distorted because of the engagement of the carboxyl hydroxyl group in a hydrogen bond with the amine hydrogen of the neighboring amide group (see Figure 2A). The calculated B3LYP/6-31G (d,p) intramolecular hydrogen bonding length (r_{GM} in Chart 1) in **1GM**–**15GM** was found in the range of 1.50–1.82 Å, and that for the hydrogen bond angle ε ($O_1H_2O_3$ in Chart 1) in the range of 143.6–172.4°. On the other hand, the DFT calculated r_{GM} and ε for **ProD 1**–**4** were 3.72–4.04 Å and 39.3–53.1°, respectively. In addition, the calculated values for angles α and β in **1GM**–**15GM** and **ProD 1GM**–**4GM** were in the range of 119.6–130.9° and 120.6–133.7°, respectively. Inspection of Table 1 indicates that the calculated values for the interatomic distance between the carboxyl hydroxyl oxygen and the amide carbonyl carbon (r_{AP}, Chart 1) range between 2.69 and 3.20 Å, whereas the value range of the angle of attack θ (Chart 1) was 49.7–104.1°.

Transition-state geometries for the tetrahedral intermediate formation (TS_2)

The calculated DFT-optimized structures for the transition states of the tetrahedral intermediate formation in **1**–**15** and **ProD 1**–**4** (**$1TS_2$**–**$15TS_2$**, **ProD $1TS_2$**–**ProD $4TS_2$**) are summarized in Table 2 and those of **$10TS_2$**–**$15TS_2$**, **ProD $1TS_2$**–**ProD $4TS_2$** are illustrated in Figures 1B and 2B, respectively. Examination of the properties of the optimized geometries of the transition states (**TS_2**) demonstrated that all of them resemble that of the corresponding GM. The calculated O–C distance in all the transition states was 2.30 Å. The angles α and β were quite similar to that of the corresponding GM structures. The values of the α angle in **$1TS_2$**–**$15TS_2$** were found in the range 113.8–123.1°, and those of the β were in the range 115.7–118.9°. On the other hand, the calculated α and β values for **ProD $1TS_2$**–**ProD $4TS_2$** were in the range 113.4–119.8° and 117.2–119.0°, respectively.

Tetrahedral intermediate geometries (INT_2)

The calculated parameters for the tetrahedral intermediate structures of **1–15** (**$1INT_2$**–**$15INT_2$**) and **ProD $1INT_2$**–**$4INT_2$** are shown in Figures 1C and 2C and are listed in Table 1. Careful inspection of the values in Table 1 revealed that angles α and β values in the intermediates are reduced when compared to that of the corresponding reactants. The α values were found in the range 107.2–110.7°, whereas for the β values the range was 107.2–111.4°. Furthermore, the angles around the tetrahedral carbon were in the range for similar regular tetrahedral intermediates.

Transition-state geometries for the tetrahedral intermediate dissociation (TS_3)

The calculated DFT geometries for the transition state of the tetrahedral intermediate dissociation step in **1**–**15 and ProD 1–4** (**$1TS_3$**–**$15TS_3$** and **ProD $1TS_3$**–**ProD $4TS_3$**, respectively) resemble that of the corresponding tetrahedral intermediates. The angle α and β values are quite identical in both the tetrahedral intermediates and their corresponding transition states. The α val-

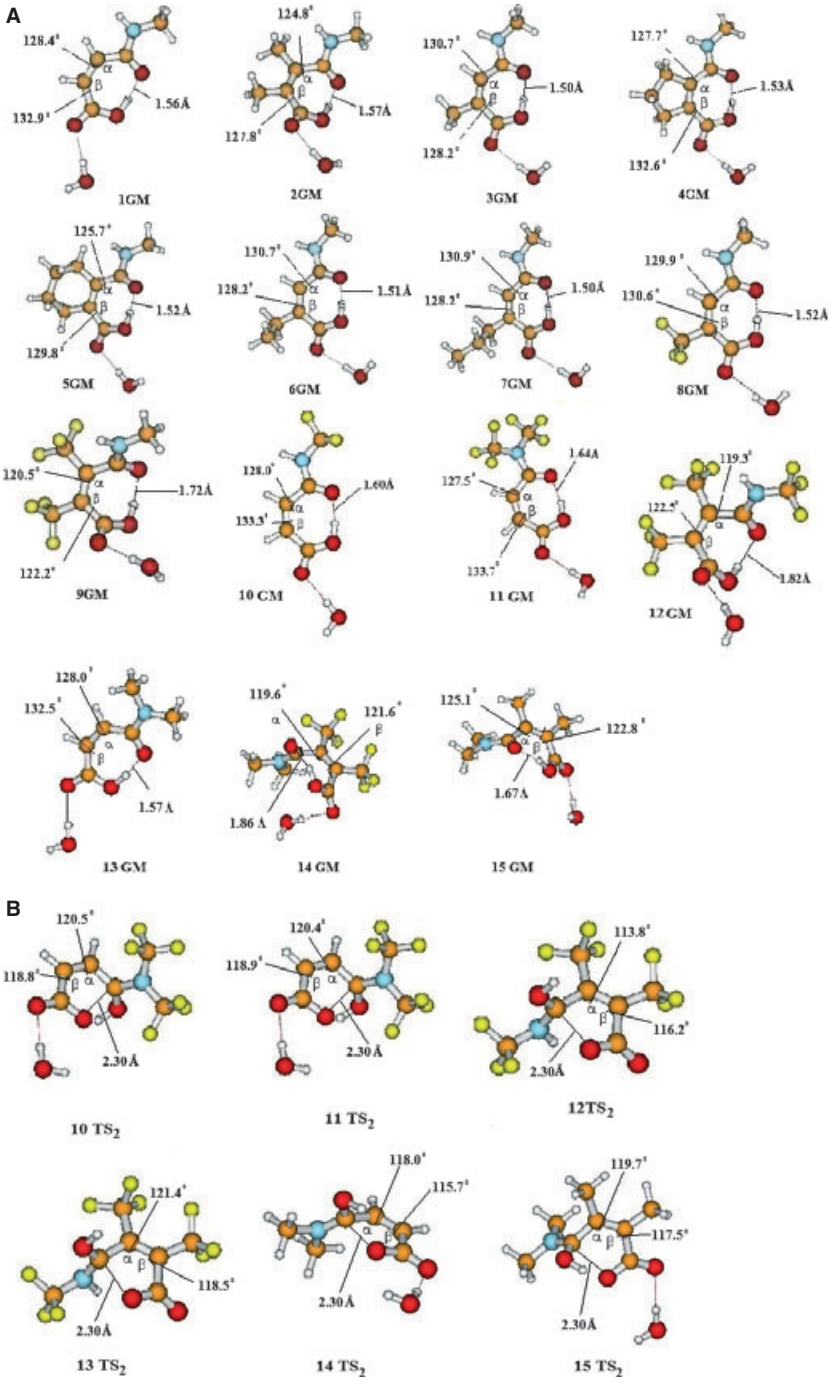

Figure 1: (A) Density functional theory (DFT)-optimized structures for **1GM**–**15GM**. (B) DFT-optimized structures for **10TS$_2$**–**15TS$_2$**. (C) DFT-optimized strucures for **1INT$_2$**–**15INT$_2$**. GM, global minimum structures. For Cartesian co-ordinates for optimized structures see Appendix S1.

ues were found in the range 107.0–108.4°, and values of the β were in the range 108.3–109.2°.

Mechanistic investigation

The DFT at B3LYP/6-31G (d,p) level of theory kinetic and thermodynamic properties for all possible routes for the acid-catalyzed hydrolysis reactions of acid amides **1**–**15** and **ProD 1–4** (Scheme 4) were calculated using the quantum chemical package Gaussian-98[a].

The enthalpy and entropy energy values for all entities involved in the hydrolysis (GM, products (P), transition states, TS_1, TS_2, and TS_3, and intermediates, INT_1, INT_2, and INT_3) were calculated in the gas phase

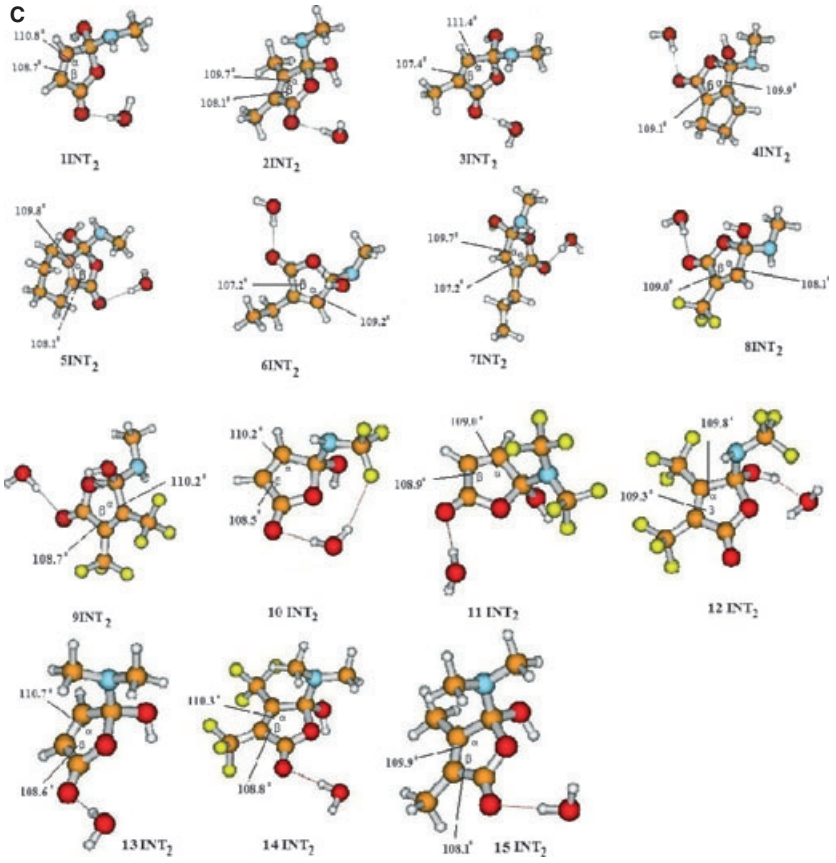

Figure 1: (*Continued*)

and water. Table 2 lists the energy values for **1GM**–**15GM**, **ProD 1GM**–**ProD 4GM**, **1INT$_2$**–**15INT$_2$**, **ProD 1INT$_2$**, **ProD 4INT$_2$**, **10TS$_2$**–**15TS$_2$**, **1TS$_3$**–**9TS$_3$**, **ProD 1TS$_2$**, and **ProD 4TS$_2$**. Figures 1A–C and 2A–C show the DFT-optimized structures for some of the GM, INT_2, TS_2, and TS_3 in **1**–**15** and **ProD 1–4**.

Using the calculated DFT values for the enthalpy and entropy of the GM and the transition states in the hydrolysis of **1**–**15** and **ProD 1–4**, the barriers ($\Delta G^{\ddagger}$) for all steps described in Scheme 4 were calculated in the gas phase, in dielectric constant of 4.5 (ether) as well as in a dielectric constant of 78.39 (water). The activation energy values for those barriers are summarized in Tables 3 and 4. Inspection of the $\Delta G_F^{\ddagger}$, activation energy for the tetrahedral intermediate formation and $\Delta G_B^{\ddagger}$, for that of the tetrahedral intermediate breakdown) values listed in Tables 3 and 4 demonstrated that the rate-limiting step in the acid-catalyzed hydrolysis of **1**–**15** and **ProD 1–4** is dependent on three factors: (i) the alkyl substituents on the C–C double bond, (ii) the medium by which the calculations were made, and (iii) the *N*-alkyl substituent.

The factors affecting the hydrolysis rate

The substituents on the C–C double bond

In order to assign the factors affecting the reaction rate in systems **1**–**15** and **ProD 1**–**4**, it will be a must to assign first the rate-limiting step for the whole process. A careful inspection of Table 3 indicates that the gas-phase calculated free activation energies for the formation step ($\Delta G_{FGP}^{\ddagger}$) are much higher than that of the corresponding energies for the dissociation step ($\Delta G_{BGP}^{\ddagger}$). This demonstrates that the rate-limiting step in apolar solvents is the one by which a tetrahedral intermediate is formed (Scheme 4). When comparing the reactivities of the acid amides having the same *N*-alkyl group (systems **1**–**9**), an interesting observation is emerged which indicates the existence of two significant trends in the reactivity versus the structural features of the ground-state structure. These two structural parameters are the distance between the carboxyl oxygen and the amide oxygen in the reactant, r_{AP} (Chart 1), and the attack angle θ (Chart 1). As shown in Table 3, systems having reactants with short r_{AP} and large θ values are more reactive than those with long r_{AP} and small θ values. For example, the distance for the unsubstituted maleamic acid amide **1** is 3.16 Å with activation energy ($\Delta G_{FGP}^{\ddagger}$) of 33.53 kcal/mol, whereas for the dimethyl-substituted derivative **2**, the distance and $\Delta G_{FGP}^{\ddagger}$ are 3.05 Å and 27.08 kcal/mol, respectively. In fact, when the values of r_{AP} and θ were examined for correlation with the gas phase and water calculated free activation energies ($\Delta G_B^{\ddagger}$), good correlations with correlation coefficient of R = 0.84–0.90 were obtained (Figure 3A,B).

In order to shed light on the factor determining the values of the distance between the two reactive centers (r_{AP}) and the angle of attack θ, which are the two parameters responsible for the unusual

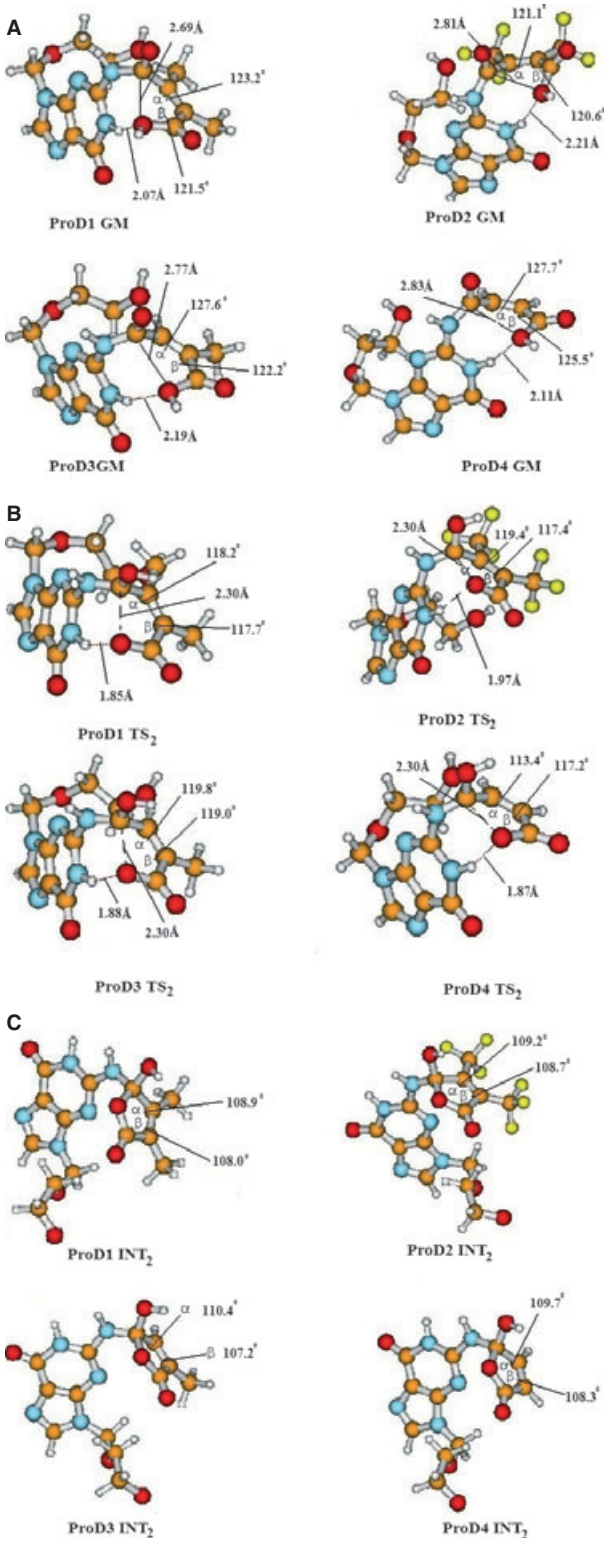

Figure 2: (A) Density functional theory (DFT)-optimized structures for **ProD 1GM**–**ProD 4GM**. (B) DFT-optimized structures for **ProD1 TS_2**–**ProD4 TS_2**. (C) DFT-optimized structures for **ProD1 INT_2**–**ProD4 INT_2**. GM, global minimum structures.

accelerations in rate for some of the derivatives such as system **2**, we have calculated, using Allinger's MM2 method (50), the strain energy values for the reactants (GM), intermediates (INT_2), and products (P) in **1–15** and **ProD 1**–**4**. The MM2 strain energies (E_s) for these structures are listed in Table 4. The MM2 calculated E_s (INT-GM) values were examined for correlation with the experimental and water calculated activation energies (Table 4). Strong correlation with a correlation coefficient $R = 0.94–0.97$ was obtained. In addition, good correlation was found between the activation energies and the strain energies of the intermediates (E_s (INT_2)). The results shown in Figure 3C indicate that the rate of the reaction for systems having small difference in the strain energies of their intermediates and corresponding reactants such as **2** and **5** is higher than that having larger values such as **1** and **4**. This might be attributed to the fact that the transition-state structures in **1**–**9** resemble those of the corresponding intermediates (Figure 3C).

Furthermore, the effect of the C–C double bond substituents on the reactivity of the acid amide was also investigated. Examination of Tables 3 and 4 indicates that the substituents have an effect on both the tetrahedral intermediate formation and its collapse. In order to test whether the substituent on the double bond has the same effect on the tetrahedral intermediate formation and the tetrahedral intermediate collapse, the DFT calculated activation energies in the gas phase and in water for the formation of the tetrahedral intermediate ($\Delta G_F^{\ddagger}$) were correlated with the energy values needed for its collapse ($\Delta G_B^{\ddagger}$). The correlation results illustrated in Figure 3D indicate strong correlations with a correlation coefficient $R = 0.92$ and 0.95, respectively. The linear correlation indicates that the driving force for the formation and collapse of the tetrahedral intermediate is the same and the rate of the acid-catalyzed hydrolysis is dependent on strain effects.

The combined results might be able to test some theories such as Koshland's 'orbital steering' and Bruice's and Menger's 'proximity orientation' that were invoked to account for rate accelerations in intramolecular and enzymatic processes.

The solvent (medium) effect

Careful examination of the energy data listed in Tables 3 and 4 reveals that while the rate-limiting step (higher barrier) in the gas phase for all systems studied (**1**–**15** and **ProD 1**–**4**) is the formation of the tetrahedral intermediate (the free activation energy for the tetrahedral intermediate formation is about 0.5–15 kcal/mol higher than that for its breakdown), the picture in water and ether is somewhat different.

For systems **1**–**9**, the rate-limiting step in water is the collapse of the tetrahedral intermediate (energy difference between the collapse and formation barriers is 2–7 kcal/mol), whereas in processes **10**–**15** and **ProD 1**–**4,** the formation of the tetrahedral intermediate is the step that determines the rate of the hydrolysis reaction (energy difference between the formation and collapse barriers is 5–30 kcal/mol). Inspection of Tables 3 and 4 and Scheme 4 revealed that the step most powerfully affected by structural changes and solvent effects is the ring closure of INT_1 to yield the

Table 1: Density functional theory (B3LYP) calculated geometries for GM, INT_2, and TS_2 in **1–15** and **ProD 1–4**

System	α in GM	β in GM	α in INT_2	β in INT_2	α in TS_2	β in TS_2	θ in GM	r_{AP} in GM	r_{GM} in GM	ε in GM
1	128.4	132.9	108.7	110.8	121.2	118.4	50.3	3.16	1.56	170.5
2	124.8	127.8	108.1	109.7	119.8	117.7	53.0	3.05	1.53	160.7
3	130.7	128.2	107.4	111.4	123.0	116.7	51.0	3.10	1.50	172.4
4	127.7	132.6	109.1	109.9	118.7	119.7	49.8	3.15	1.53	170.5
5	125.7	129.8	108.1	109.8	118.1	119.2	51.6	3.09	1.52	167.2
6	130.7	128.2	107.2	109.2	123.0	116.6	51.4	3.09	1.51	167.9
7	130.9	128.2	107.2	109.7	123.1	116.5	51.1	3.09	1.50	170.9
8	129.9	130.6	109.0	108.1	121.8	118.5	51.0	3.11	1.51	172.1
9	120.5	122.2	108.7	110.2	118.5	117.4	56.8	3.05	1.72	143.6
10	128.0	133.3	110.2	108.5	120.5	118.8	51.2	3.17	1.60	169.0
11	127.5	133.7	109.0	108.9	120.4	118.9	51.3	3.20	1.64	167.1
12	119.3	122.5	109.8	109.3	113.8	116.2	56.4	3.10	1.82	138.2
13	128.0	133.5	110.7	108.6	121.4	118.5	49.7	3.19	1.57	169.0
14	119.6	121.6	110.3	108.8	118.0	115.7	67.9	2.89	1.80	146.1
15	122.8	125.1	109.9	108.1	119.7	117.5	63.2	2.92	1.67	155.9
ProD 1	123.2	121.5	108.9	108.0	118.2	117.7	103.5	2.69	3.81	44.8
ProD 2	121.1	120.6	109.2	108.7	119.4	117.4	99.3	2.81	3.72	53.1
ProD 3	127.6	122.2	110.4	107.2	119.8	119.0	101.2	2.77	3.87	43.6
ProD 4	127.7	125.5	109.7	108.3	113.4	117.2	104.1	2.83	4.04	39.3

B3LYP refers to values calculated by B3LYP/6-31G (d, p) method. GM, INT_2, and TS_4 refer to global minimum, intermediate, and transition-state structures, respectively (see Scheme 4). For the definition of the bond angles α, β, θ, and ε and distances r_{GM} and r_{AP}, see Chart 1. The angle unit is degree and the r_{GM} and r_{AP} unit is Å.

tetrahedral intermediate INT_2. Examination of the geometries of the transition states for this step (TS_2) indicates that TS_2 is in the ionic form. It is expected that the effect of polar solvents on the stability of TS_2 will be different from that of solvents with less polarity. The free activation energies for the approach process ($\Delta G_F^{\ddagger}$) and the dissociation process ($\Delta G_B^{\ddagger}$) calculated in the gas phase, ether and in presence of water listed in Tables 3 and 4 indicate that solvents with low dielectric constant such as in the case of the gas phase tend to shift the equilibrium to the reactants by destabilizing TS_2, making the approach step as the rate limiting, whereas solvents with high dielectric constants such as water interact strongly with the ionic transition state to affect the equilibrium to be shifted to the right side. These interactions stabilize the approach transition state (TS_2) and consequently lower the approach barrier, hence making the reaction rate dependent on the dissociation step. A representation of the energy profiles for the hydrolysis of **ProD 1** and **2** as calculated in water is illustrated in Figure 4.

On the other hand, when comparing the effect of ether as a solvent on the reaction rates of **1**–**9**, the DFT calculation results indicate that in the presence of ether (dielectric constant = 4.5), the rate-limiting step in systems **2** and **5** is the formation of the tetrahedral intermediate, whereas in the other processes the rate-limiting step is the dissociation of the tetrahedral intermediate (see Tables 3 and 4).

The *N*-alkyl substituent

In order to study the role of the leaving group on the mode and the nature of the intramolecular acid-catalyzed hydrolysis mechanism of acid amides systems having different leaving groups (groups with different p*K*a and bulkiness), systems **10**–**15** were computationally investigated and their calculated properties were compared to those for **1**–**9**. Compounds **10**–**15** represent different systems by which the leaving group NHMe is replaced with more or less basic leaving groups. Compounds **10**–**12** are examples of systems having less basic leaving groups ($NHCF_3$ and $N(CF_3)_2$), whereas compounds **13**–**15** represent those with more basic leaving group ($N(Me)_2$). The DFT calculation results revealed that the rate-limiting step in **10–15** is the formation of the tetrahedral intermediate and not its collapse as observed with systems **1**–**9**. In addition, the energy difference between the two barriers (the formation and collapse) was largely affected by the nature of the leaving group. For example, the higher barrier in system **1** was the collapse step and the energy difference between the collapse and the formation barriers was about 7 kcal/mol, whereas in systems **10** and **11** which are similar to **1** except that the leaving group in **10** is $NHCF_3$ and in **11** is $N(CF_3)_2$, the rate-limiting step was the formation of the tetrahedral intermediate and the energy difference between the two barriers was −4.4 kcal/mol for **10** and −17.4 kcal/mol for **11**. Furthermore, when the leaving group in **1** was replaced with $N(Me)_2$ such as in **13**, the energy difference between the two barriers was about −5.5 kcal/mol. Furthermore, strong correlation was obtained when the strain energy difference between the intermediates and the corresponding reactants (E_s INT-GM) was plotted against the water free activation energy of systems **10**–**15** and **ProD 1**–**4** with a correlation coefficient of $R = 0.90$. This indicates that in addition to other effects, strain effect has a profound effect on the rates of the reactions in **10**–**15** and **ProD 1**–**4**.

The combined results suggest that both the p*K*a and the volume of the leaving group have a significant effect on determining the rate-limiting step and the magnitude of the barriers. In systems with trifluoromethylamine and di-trifluoromethylamine leaving groups, the ratio of the tetrahedral intermediate formation to collapse barriers

Table 2: Density functional theory (B3LYP/6-31G (d,p)) calculated properties for the acid-catalyzed hydrolysis of acid amides **1–15**, **ProD 1–4,** and **Inter**

Compound	Enthalpy, H (gas phase) In Hartree	Entropy, S (gas phase) Cal/Mol-Kelvin	Frequency (/cm)	MM2Es kcal/mol
1GM	−551.6209552	115.71	–	10.16
1INT$_2$	−551.5899873	113.12	–	20.55
1TS$_3$	−551.9510979	100.58	29.18i	–
2GM	−630.2556684	133.45	–	10.82
2INT$_2$	−630.2424070	125.08	–	16.16
2TS$_3$	−630.6125865	117.89	57.26i	–
3GM	−590.9452364	126.16	–	9.40
3INT$_2$	−590.9162845	124.52	–	17.32
3TS$_3$	−591.284155	109.50	45.91i	–
4GM	−668.3716758	131.90	–	12.30
4INT$_2$	−668.3272626	125.09	–	27.89
4TS$_3$	−668.7001822	116.95	73.72i	–
5GM	−707.6805570	136.69	–	9.18
5INT$_2$	−707.6689275	122.73	–	19.25
5TS$_3$	−707.6321442	122.88	118.05i	–
6GM	−630.2606708	132.74	–	5.12
6INT$_2$	−630.2326178	132.45	–	17.59
6TS$_3$	−630.60156591	116.93	52.77i	–
7GM	−669.5780833	138.31	–	6.20
7INT$_2$	−669.5495044	137.75	–	18.55
7TS$_3$	−669.9185072	124.96	68.64i	–
8GM	−888.6478787	140.60	–	12.86
8INT$_2$	−888.6201859	137.62	–	22.34
8TS$_3$	−888.9742696	120.84	37.75i	–
9GM	−1225.6575172	145.62	–	28.29
9INT$_2$	−1225.6422023	147.77	–	26.92
9TS$_3$	−1225.9938255	140.05	33.82i	–
10GM	−849.3302758	134.63	–	14.15
10INT$_2$	−849.3095129	114.95	–	21.56
10TS$_2$	−849.2721283	122.84	92.14i	–
11GM	−1186.3372601	145.78	–	25.52
11INT$_2$	−1186.3271376	136.12	–	19.78
11TS$_2$	−1186.2730867	135.57	148.15i	–
12GM	−1523.3652973	163.37	–	35.90
12INT$_2$	−1523.3731299	154.94	–	28.25
12TS$_2$	−1523.3352867	149.02	119.78i	–
13GM	−590.9248107	112.69	–	13.43
13INT$_2$	−590.8983010	121.16	–	26.54
13TS$_2$	−590.9074094	117.48	171.92i	–
14GM	−1264.9706324	153.57	–	15.58
14INT$_2$	−1264.9515630	152.18	–	33.55
14TS$_2$	−1264.9379165	151.77	99.37i	–
15GM	−669.5621811	139.20	–	7.13
15INT$_2$	−669.5503948	131.65	–	24.71
15TS$_2$	−669.5259892	134.31	108.02i	–
ProD1 GM	−1268.8689365	172.98	–	32.70
ProD1 INT$_2$	−1268.8710712	171.06	–	29.45
ProD1 TS$_2$	−1268.8183062	169.43	134.62i	–
ProD2 GM	−1864.2702113	193.14	–	48.80
ProD2 INT$_2$	−1864.2731292	190.94	–	42.27
ProD2 TS$_2$	−1864.2190556	186.37	79.43i	–
ProD3 GM	−1229.5483175	164.26	–	35.70
ProD3 INT$_2$	−1229.5446492	162.24	–	31.16
ProD3 TS$_2$	−1229.5029859	157.29	92.96i	–
ProD4 GM	−1190.2238966	161.03	–	36.05
ProD4 INT$_2$	−1190.2183473	156.05	–	34.64
ProD4 TS$_2$	−1190.1752961	149.14	102.40i	–
InterGM	−631.4579281	141.61	–	2.98
InterINT$_2$	−631.4282861	129.50	–	13.64
InterTS$_3$	−631.7933134	130.70	57.27i	–

GM, INT, and TS are global minimum, intermediate, and transition-state structures, respectively. MM2Es is the strain energy calculated by Allinger's MM2 method.

is much higher than in the cases where methylamine and di-methylamine are the leaving group. This might be attributed to the fact that trifluoromethyl group is an electron-withdrawing group that makes the amine moiety a good leaving group in the dissociation process of the tetrahedral intermediate. Hence, the formation/collapse barriers ratio is shifted toward the formation, whereas in the cases where the leaving group is $NHCH_3$ or $N(CH_3)_2$, the amine moiety has less ability to leave because of the electron-donating effect of the methyl group. This result is in accordance with the conclusions drawn by Kluger and Chin (47).

DFT calculated reaction rates versus experimental values

For drawing credibility to the DFT calculations executed in this study, the water calculated B3LYP/6-31G(d,p) free activation energies for the tetrahedral intermediate collapse ($\Delta G^{\ddagger}_{BW}$) were correlated with the corresponding experimental free activation energies (Exp $\Delta G^{\ddagger}$). Strong correlation was obtained with a correlation coefficient $R = 0.95$ (Figure 5A).

In order to confirm that the DFT calculations at B3LYP/6-31G (d,p) level of theory are not dependent on the specific theoretical method used, the kinetic and thermodynamic properties for processes **1**–**3** were calculated at a higher level, B3LYP/311 + G (d,p)[a], and with hybrid GGA (MPW1k) functional (39) as well. The energy data calculated by the three different methods were examined for correlation. Strong correlation was found between the examined values with a correlation coefficient of $R = 0.99$.

The effective molarities (EM) for processes 1–15 and ProD 1–4

The effective molarity (EM) parameter is commonly used as a measure for intramolecular efficiency. It is defined as a rate ratio of the intramolecular reaction and its corresponding intermolecular where both reactions are driven by the same mechanism. The main factors determining the EM parameter are ring size, solvent, and reaction type. Cyclization reactions through intramolecular nucleophilic addition are much more efficient than intramolecular proton transfers. Values in the order of 10^9–10^{13} M have been measured for the EM in intramolecular processes occurring through nucleophilic addition, whereas for proton-transfer processes EM values of <10 M were obtained (51).

Table 3: Density functional theory (B3LYP) calculated kinetic and thermodynamic properties in the gas phase for the acid-catalyzed hydrolysis of **1–15**, **ProD 1–4,** and **Inter**

System	$\Delta H^{\ddagger}_{BGP}$ (kcal/mol)	$T\Delta S^{\ddagger}_{BGP}$ (kcal/mol)	$\Delta G^{\ddagger}_{BGP}$ (kcal/mol)	$\Delta H^{\ddagger}_{FGP}$ (kcal/mol)	$T\Delta S^{\ddagger}_{FGP}$ (kcal/mol)	$\Delta G^{\ddagger}_{FGP}$ (kcal/mol)	$\Delta G^{\ddagger}_{Bether}$ (kcal/mol)	$\Delta G^{\ddagger}_{Fether}$ (kcal/mol)
1	27.31	−0.77	28.08	32.46	−1.09	33.53	34.27	31.35
2	13.93	−2.49	16.42	25.67	−1.41	27.08	16.32	21.29
3	24.41	−0.49	24.90	30.68	−1.89	32.57	29.53	28.23
4	34.42	−2.35	36.77	41.88	−3.49	45.37	40.23	39.27
5	13.25	−4.16	17.41	24.55	−2.32	26.87	18.51	22.34
6	23.83	−0.09	23.92	30.11	−2.01	32.12	29.53	27.50
7	24.86	−0.17	25.03	30.76	−1.54	32.30	28.35	27.76
8	24.08	−0.89	24.87	29.79	−2.58	32.37	–	–
9	17.88	0.64	17.24	24.17	−1.77	25.94	–	–
10	13.66	−5.86	19.52	36.49	−3.51	40.00	–	–
11	15.06	−2.88	17.94	40.27	−3.04	43.31	–	–
12	0	−2.51	2.51	18.83	−4.28	23.11	–	–
13	22.91	2.52	20.39	27.62	1.43	26.19	–	–
14	19.54	−0.44	19.98	20.53	−0.54	21.07	–	–
15	13.04	−2.25	15.29	22.71	−1.46	24.27	–	–
ProD 1	4.08	−0.57	4.65	31.77	−1.06	32.83	–	–
ProD 2	0	−0.66	0.66	32.10	−2.02	34.12	–	–
ProD 3	2.20	−0.60	2.80	28.45	−2.08	30.53	–	–
ProD 4	3.45	−1.48	4.93	30.50	−3.54	34.04	–	–
Inter	39.90	−3.35	43.25	–	–	–	–	–

B3LYP refers to values calculated by B3LYP/6-31G (d, p) method. $\Delta H^{\ddagger}$ is the calculated activation enthalpic energy (kcal/mol). $T\Delta S^{\ddagger}$ is the calculated activation entropic energy (kcal/mol). $\Delta G^{\ddagger}$ is the calculated activation free energy (kcal/mol). B and F refer to tetrahedral intermediate breakdown and tetrahedral intermediate formation. GP and ether refer to calculated in the gas phase and in ether, respectively.

Table 4: Density functional theory (DFT) (B3LYP) calculated kinetic and thermodynamic properties for the acid-catalyzed hydrolysis of **1–15**, **ProD 1–4,** and **Inter**

System	$\Delta H^{\ddagger}_{BW}$ (kcal/mol)	$\Delta G^{\ddagger}_{BW}$ (kcal/mol)	log k_{rel} (36)	Log EM (36) (Exp)	Log EM (Calc)	E_s (INT_2) (kcal/mol)	E_s (P) (kcal/mol)	E_s (GM) (kcal/mol)	$\Delta H^{\ddagger}_{FW}$ (kcal/mol)	$\Delta G^{\ddagger}_{FW}$ (kcal/mol)
1	32.29	33.06	0	7.724	8.52	20.55	25.08	10.16	25.01	26.10
2	17.56	20.05	4.371	15.86	18.08	16.16	18.93	10.82	16.49	17.90
3	27.93	28.42	1.494	7.742	11.93	17.32	21.70	9.40	22.91	24.80
4	35.76	38.11	−4.377	1.255	4.81	27.89	32.75	12.30	28.67	32.16
5	18.96	23.12	2.732	15.190	15.82	19.25	23.13	9.18	15.57	17.89
6	27.19	27.28	1.516	6.962	12.76	17.59	22.95	5.12	21.86	23.87
7	27.38	27.55	1.648	8.568	12.57	18.55	24.00	6.20	22.86	24.40
8	29.23	30.12	–	–	6.36	22.34	27.77	12.86	21.08	23.66
9	15.79	15.15	–	–	21.68	26.92	35.64	28.29	10.20	11.97
10	18.76	24.64	–	–	11.47	26.92	35.64	28.29	25.53	29.04
11	16.14	19.02	–	–	6.06	21.56	25.08	14.15	33.37	36.41
12	6.28	8.79	–	–	16.01	19.78	25.08	25.52	18.59	22.87
13	15.94	13.42	–	–	18.75	28.25	35.64	35.90	20.66	19.13
14	14.85	15.29	–	–	21.28	26.54	25.08	13.43	15.16	15.70
15	12.79	15.04	–	–	20.49	33.55	35.64	15.58	15.32	16.78
ProD 1	1.57	2.07	–	–	13.36	24.71	–	7.13	25.40	26.46
ProD 2	0	0.66	–	–	9.66	29.45	–	32.70	29.48	31.50
ProD 3	1.26	2.26	–	–	15.94	42.27	–	48.80	20.88	22.96
ProD 4	0.94	2.92	–	–	13.91	31.16	–	35.70	22.19	25.73
Inter	41.30	44.65	–	–	–	13.64	12.10	–	–	–

EM, effective molarities; GM, global minimum structures.

B3LYP refers to values calculated by B3LYP/6-31G (d, p) method. $\Delta H^{\ddagger}$ is the calculated activation enthalpic energy (kcal/mol). $T\Delta S^{\ddagger}$ is the calculated activation entropic energy (kcal/mol). $\Delta G^{\ddagger}$ is the calculated activation free energy (kcal/mol). E_s refers to strain energy calculated by Allinger's MM2 method (50). INT_2 and P refer to intermediate 2 and product, respectively. $\mathbf{EM} = \mathbf{exp} - (\Delta G^{\ddagger}_{inter} - \Delta G^{\ddagger}_{intra})/RT$. BW and FW refer to tetrahedral intermediate breakdown and tetrahedral intermediate formation calculated in water, respectively. Exp refers to experimental value. Calc refers to DFT calculated values.

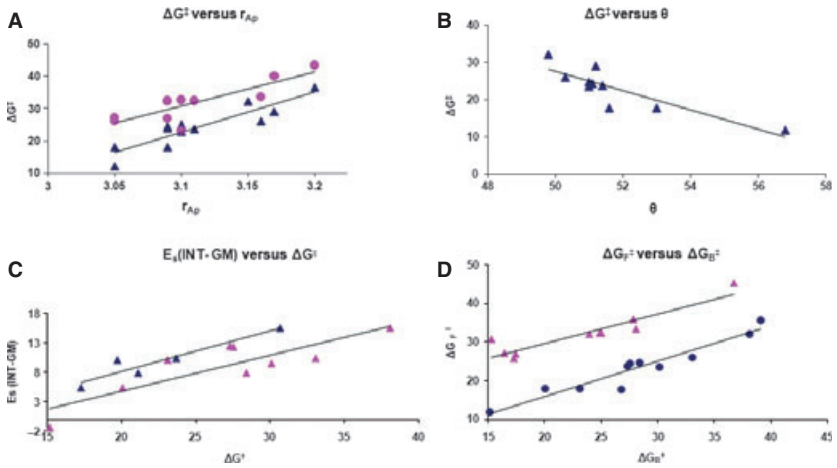

Figure 3: (A) Plot of $\Delta G^{\ddagger}$ versus r_{AP} in **1**–**9**, where the blue points for the calculated density functional theory (DFT) values (in water) and the pink points for the gas-phase calculated values. (B) Plot of $\Delta G^{\ddagger}$ versus θ in **1**–**9**, where the blue points for the water calculated DFT values and the pink points for the gas-phase calculated values. (C) Plot of E_s (INT-GM) versus $\Delta G^{\ddagger}$ in **1**–**9**, where the blue points for the experimental values and the pink points for the water calculated DFT values. (D) Plot of $\Delta G_F^{\ddagger}$ versus $\Delta G_B^{\ddagger}$ in **1**–**9**, where the blue points for the water DFT calculated values and the pink points for the gas-phase DFT calculated values. r_{AP} is the distance between the hydroxyl oxygen of the carboxylic group and the carbon of the amide carbonyl in the reactant. θ is the angle of attach of the approach of the carboxylic hydroxyl group toward the amide carbonyl carbon in the reactant. E_s is strain energy, $\Delta G^{\ddagger}$ is the free activation energy. $\Delta G_F^{\ddagger}$ and $\Delta G_B^{\ddagger}$ refer to the free activation energy for the tetrahedral intermediate formation and collapse, respectively.

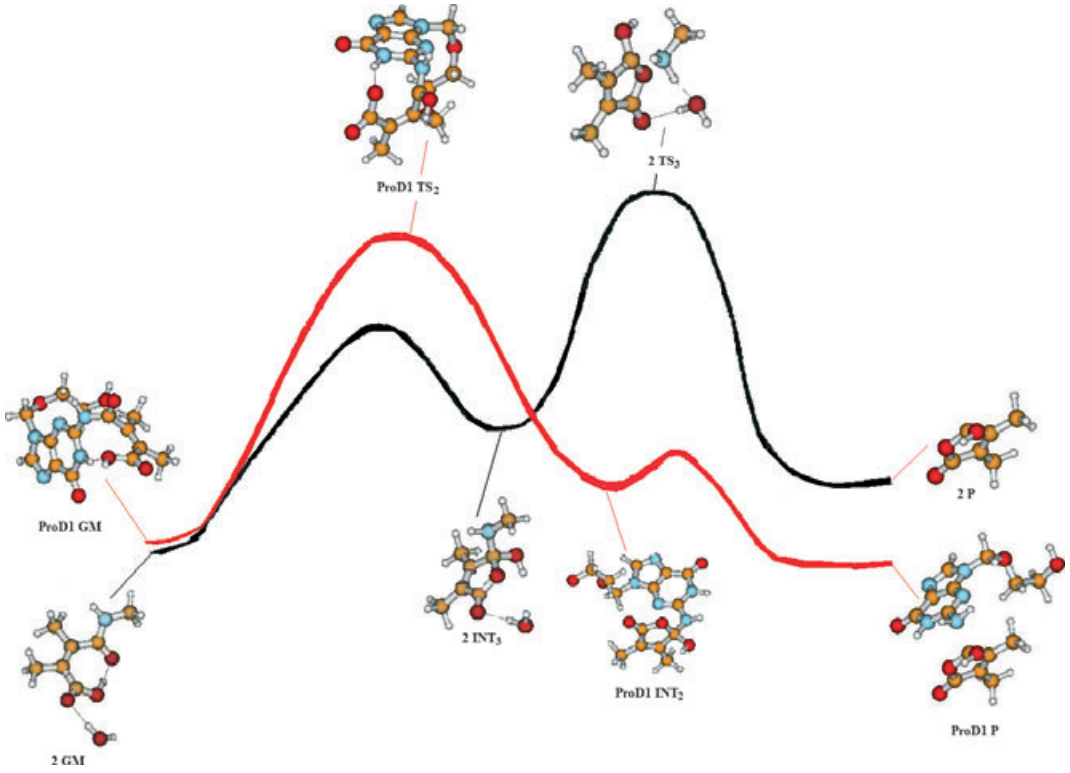

Figure 4: A representation of an energy profile for acid-catalyzed hydrolysis of **ProD 1** and **2** as calculated in water. GM. TS, INT, and P refer to global minimum, transition-state, intermediate, and product structures, respectively. TS_2 and TS_3 are approach and dissociation transition-state structures, respectively.

For obtaining the EM values for processes **1**–**15** and **ProD 1**–**4**, we have calculated the kinetic and thermodynamic parameters for their corresponding intermolecular process, **Inter** (Scheme 5).

Using eqns 1–4, eqn 5 was derived. Equation 5 describes the EM term as a function of the difference in the activation energies of the intramolecular process and the corresponding

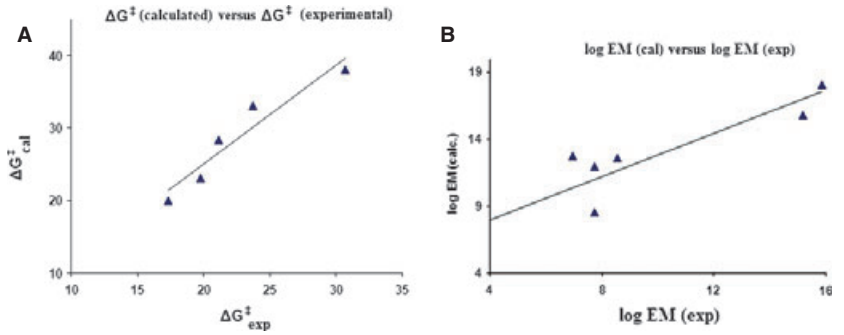

Figure 5: (A) Plot of $\Delta G^{\ddagger}$ (Calculated) versus $\Delta G^{\ddagger}$ (Experimental) in **1**–**9**. $\Delta G^{\ddagger}$ (Calculated) and $\Delta G^{\ddagger}$ (Experimental) are the water calculated density functional theory (DFT) free activation energy and experimental free activation energy, respectively. (B) log EM (calc) versus log EM (exp) in **1**–**9**. EM refers to effective molarity; calc and exp refer to calculated by DFT and experimental, respectively.

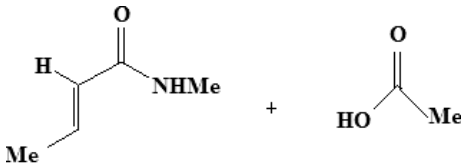

Inter

Scheme 5: Corresponding intermolecular reaction for **1**–**15** and **ProD1**–**4**.

intermolecular processes. The calculated EM values for processes **1**–**15** and **ProD 1**–**4** as calculated by eqn 5 are listed in Table 4.

$$EM = k_{intra}/k_{inter} \quad (1)$$

$$\Delta G^{\ddagger}_{inter} = -RT\ln k_{inter} \quad (2)$$

$$\Delta G^{\ddagger}_{intra} = -RT\ln k_{intra} \quad (3)$$

$$\Delta G^{\ddagger}_{intra} - \Delta G^{\ddagger}_{inter} = -RT\ \ln k_{intra}/k_{inter} \quad (4)$$

$$\ln EM = -(\Delta G^{\ddagger}_{intra} - \Delta G^{\ddagger}_{inter})/RT \quad (5)$$

where T is the temperature in Kelvin and R is the gas constant.

The calculated log EM values in Table 4 were correlated with the corresponding EM experimental values. The correlation equation with its correlation coefficient is shown in Figure 5B and eqn 6. Careful examination of the calculated log EM values listed in Table 4 and Figure 5B demonstrated that **2**, **5**, and **13**–**15** were the most efficient processes among **1**–**15**, whereas process **4**, **8**, and **11** were the least. The discrepancy in rates between **2**, **5**, and **13**–**15** on the one hand and **4**, **8**, and **11** on the other hand is attributed to strain effects.

The calculated and experimental EM values were found to be comparable; however, there is a discrepancy in their absolute values. This might be due to the fact that the EM experimental measurement for the systems studied was taken in the presence of aqueous acid medium, whereas the DFT calculations were made in plain water. The dielectric constant value for a mixture of acid/water is expected to be different from that of water (78.39) and hence the discrepancy in the calculated and experimental EM values[b].

$$\log EM\ (\text{calculated}) = -0.809 \log EM\ (\text{experimental}) + 4.75 \quad R^2 = 0.86 \quad (6)$$

Calculation of the $t_{1/2}$ values for the acid-catalyzed hydrolysis of prodrugs ProD 1–4

The calculated DFT properties for processes **ProD 1**–**4** including the geometries of GM, intermediate (INT_2), and transition-state (TS_2) structures are shown in Figure 2 and listed in Tables 1–4. Comparison of these calculated structures to that for processes **1**–**15** revealed a close similarity.

Using eqns 7 and 8 obtained from the correlation of log k_{rel} versus $\Delta G^{\ddagger}_{B}$ and $\Delta G^{\ddagger}_{F}$ versus $\Delta G^{\ddagger}_{B}$ and the $t_{1/2}$ value for process 2, $t_{1/2}$ = 1 second (36), we have calculated the $t_{1/2}$ values for **ProD 1**–**4**. The calculated $t_{1/2}$ values at pH 2 for **ProD 1**–**ProD 4** are 29.2 h, 6097 days, 4.6 min, and 8.34 h, respectively.

$$\log k_{rel} = -0.442\Delta G^{\ddagger}_{B} + 13.534 \quad R^2 = 0.93 \quad (7)$$

$$\Delta G^{\ddagger}_{F} = -0.798\Delta G^{\ddagger}_{B} + 1.346 \quad R^2 = 0.94 \quad (8)$$

Conclusions and Future Directions

The DFT calculations at B3LYP/6-31G(d,p) level for the acid-catalyzed hydrolysis in acid amides **1**–**15** and **ProD 1**–**4** demonstrated that the reaction proceed via four steps where the tetrahedral intermediate formation and its collapse are the two main barriers determining the rate-limiting step. The calculation results revealed that when the reaction is carried out in the gas phase or in apolar solvents, the higher barrier is the formation of the tetrahedral intermediate, whereas when the reaction medium is water or polar solvent, the rate-limiting step in processes **1**–**9** is the tetrahedral intermediate collapse and in systems **10**–**15** and **ProD 1**–**4** is

the tetrahedral intermediate formation. Furthermore, the calculations demonstrated that the efficiency of these processes is largely sensitive to the pattern of substitution on the carbon–carbon double bond and the nature of the amide *N*-alkyl group. The reaction rate was found to be linearly correlated with the following characteristics: (i) the strain energy difference between the intermediate and the reactant (E_s INT-GM), (ii) the distance between the hydroxyl oxygen of the carboxyl group and the amide carbonyl carbon (r_{AP}), and (iii) the attack angle θ by which the approach step commences. In addition, a linear correlation between the calculated and experimental EM values reinforces the credibility of using DFT methods in predicting energies as well as the rates for reactions of the type described herein.

Using the correlation equation obtained from the plot of the calculated and experimental EM values, we have calculated the $t_{1/2}$ of four different acyclovir prodrugs (**ProD 1**–**4**). The $t_{1/2}$ values of those products were dependent on the nature of the substitution on the C–C double bond.

The strategy to achieve desirable prodrugs of acyclovir that are capable of releasing acyclovir in a slow release manner is as follows: (i) synthesis of the linker and coupling of the parent drug to the linker using Kirby's synthetic procedure were carried out (36); (ii) kinetic studies (*in vitro*) of the synthesized prodrugs will be performed in physiological environment (37 °C, pH = 2.0 and 6.0 in aqueous medium); and (iii) for the prodrugs that show desirable slow release in the *in vitro* studies, *in vivo* pharmacokinetic studies will be conducted in order to determine the bioavailability and the duration of action of the tested prodrugs. In light of the *in vivo* pharmacokinetics, new prodrugs will be designed and synthesized.

It should be emphasized that further studies of factors that are not accessible to calculations should be made because the bioavailability of prodrugs **ProD1**–**ProD4** is not precisely predicted from their structures owing to the influence of physiological bases and acids that are likely to influence the overall rates and the stability of the prodrug in the acid stomach environment.

Acknowledgments

The Karaman Co. is thanked for support of our computational facilities. Special thanks are also given to Angi Karaman, Donia Karaman, Rowan Karaman, and Nardene Karaman for technical assistance.

References

1. de Clercq E., Field H.J. (2006) Antiviral prodrugs – the development of successful prodrug strategies for antiviral chemotherapy. Br J Pharmacol;147:1–11.
2. de Miranda P., Blum M.R. (1983) Pharmacokinetics of acyclovir after intravenous and oral administration. J Antimicrob Chemother;12(Suppl. B):29–37.
3. Blum M.R., Liao S.H.T., de Miranda P. (1982) Overview of acyclovir pharmacokinetic disposition in adults and children. Am J Med;73(Suppl. 1A):186–192.
4. Luengo J., Aranguiz T., Sepulveda J. (2002) Preliminary pharmacokinetic study to different preparations of acyclovir with β-cyclodextrin. J Pharm Sci;91:2593–2598.
5. Attia I.A., El-Gizawy S.A., Fouda M.A., Donia A.M. (2007) Influence of a niosomal formulation on the oral bioavailability of acyclovir in rabbits. AAPS Pharm Sci Tech; 8: Article 106. DOI: 10.1208/pt0804106.
6. Yadav S., Jain S., Prajapati S., Motwani M., Kumar S. (2011) Formulation and in vitro and in vivo characterization of acyclovir loaded mucoadhesive microspheres. J Pharm Sci Tech;3:441–447.
7. Soul-Lawton J., Seaber E., On N., Wootton R., Rolan P., Posner J. (1995) Absolute bioavailability and metabolic disposition of valaciclovir, the L-valyl ester of acyclovir, following oral administration to humans. Antimicrob Agents Chemother;39:2759–2764.
8. Tolle-Sander S., Lentz K.A., Maeda D.Y., Coop A., Polli J.E. (2004) Increased acyclovir oral bioavailability via a bile acid conjugate. Mol Pharm;1:40–48.
9. Karaman R. (2008) Analysis of Menger's spatiotemporal hypothesis. Tetrahedron Lett;49:5998–6002.
10. Karaman R. (2009) Cleavage of Menger's aliphatic amide: a model for peptidase enzyme solely explained by proximity orientation in intramolecular proton transfer. J Mol Struct;910:27–33.
11. Karaman R. (2010) The efficiency of proton transfer in Kirby's enzyme model, a computational approach. Tetrahedron Lett;51: 2130–2135.
12. Karaman R., Pascal R. (2010) A computational analysis of intramolecularity in proton transfer reactions. Org Biomol Chem; 8:5174–5178.
13. Karaman R., Hallak H. (2010) Anti-malarial pro-drugs- a computational aided design. Chem Biol Drug Des;76:350–360.
14. Karaman R. (2010) A general equation correlating intramolecular rates with attack'' parameters: distance and angle. Tetrahedron Lett;51:5185–5190.
15. Karaman R. (2010) Prodrugs of Aza nucleosides based on proton transfer reactions. J Comput Aided Mol Des;24:961–970.
16. Karaman R. (2011) Analyzing the efficiency of proton transfer to carbon in Kirby's enzyme model – a computational approach. Tetrahedron Lett;52:699–704.
17. Hejaz H., Karaman R., Khamis M. (2012) Computer-assisted design for paracetamol masking bitter taste prodrugs. J Mol Model;18:103–114.
18. Kirby A.J., Parkinson A. (1994) Most efficient intramolecular general acid catalysis of acetal hydrolysis by the carboxyl group. J Chem Soc Chem Commun;707–708.
19. Brown C.J., Kirby A.J. (1997) Efficiency of proton transfer catalysis. Intramolecular general acid catalysis of the hydrolysis of dialkyl acetals of benzaldehyde. J Chem Soc Perkin Trans;2:1081–1093.
20. Craze G.-A., Kirby A.J. (1974) The hydrolysis of substituted 2-methoxymethoxybenzoic acids. J Chem Soc Perkin Trans;2:61–66.
21. Barber S.E., Dean K.E.S., Kirby A.J. (1999) A mechanism for efficient proton-transfer catalysis. Intramolecular general acid catalysis of the hydrolysis of 1-arylethyl ethers of salicylic acid. Can J Chem;792–801.
22. Kirby A.J., de Silva M.F., Lima D., Roussev C.D., Nome F. (2006) Efficient intramolecular general acid catalysis of nucleophilic attack on a phosphodiester. J Am Chem Soc;128:16944–16952.

23. Kirby A.J., Williams N.H. (1994) Efficient intramolecular general acid catalysis of enol ether hydrolysis. Hydrogen-bonding stabilization of the transition state for proton transfer to carbon. J Chem Soc Perkin Trans;2:643–648.
24. Kirby A.J., Williams N.H. (1991) Efficient intramolecular general acid catalysis of vinyl ether hydrolysis by the neighbouring carboxylic acid group. J Chem Soc Chem Commun;1643–1644.
25. Hartwell E., Hodgson D.R.W., Kirby A.J. (2000) Exploring the limits of efficiency of proton-transfer catalysis in models and enzymes. J Am Chem Soc;122:9326–9327.
26. Kirby A.J. (1997) Efficiency of proton transfer catalysis in models and enzymes. Acc Chem Res;30:290–296.
27. Asaad N., Davies J.E., Hodgson D.R.W., Kirby A.J. (2005) The search for efficient intramolecular proton transfer from carbon: the kinetically silent intramolecular general base-catalysed elimination reaction of o-phenyl 8-dimethylamino-1-naphthaldoximes. J Phys Org Chem;18:101–109.
28. Menger F.M., Ladika M. (1990) Remote enzyme-coupled amine release. J Org Chem;35:3006–3007.
29. Menger F.M., Ladika M. (1988) Fast hydrolysis of an aliphatic amide at neutral pH and ambient temperature. A peptidase model. J Am Chem Soc;110:6794–6796.
30. Menger F.M. (1985) On the source of intramolecular and enzymatic reactivity. Acc Chem Res;18:128–134.
31. Menger F.M., Chow J.F., Kaiserman H., Vasquez P.C. (1983) Directionality of proton transfer in solution. Three systems of known angularity. J Am Chem Soc;105:4996–5002.
32. Menger F.M. (1983) Directionality of organic reactions in solution. Tetrahedron;39:1013–1040.
33. Menger F.M., Grosssman J., Liotta D.C. (1983) Transition-state pliability in nitrogen-to-nitrogen proton transfer. J Org Chem; 48:905–907.
34. Menger F.M., Galloway A.L., Musaev D.G. (2003) Relationship between rate and distance. Chem Commun;2370–2371.
35. Menger F.M. (2005) An alternative view of enzyme catalysis. Pure Appl Chem;77:1873–1876 and references therein.
36. Kirby A.J., Lancaster P.W. (1972) Structure and efficiency in intramolecular and enzymatic catalysis. Catalysis of amide hydrolysis by the carboxy-group of substituted maleamic acids. J Chem Soc Perkin Trans;2:1206–1214.
37. Kirby A.J., Hollfelder F. (2009) From Enzyme Models to Model Enzymes, 1st edn. Cambridge: Royal Society of Chemistry.
38. Casewit C.J., Colwell K.S., Rappe' A.K. (1992) Application of a universal force field to main group compounds. J Am Chem Soc;114:10046–10053.
39. Zheng J., Zhao Y., Truhlar D.G. (2009) The DBH24/08 database and its use to assess electronic structure model chemistries for chemical reaction barrier heights. J Chem Theory Comput;5:808–821.
40. Murrell J.N., Laidler K.J. (1968) Symmetries of activated complexes. Trans Faraday Soc;64:371–377.
41. Muller K. (1980) Reaction paths on multidimensional energy hypersurfaces. Angew Chem Int Ed Engl;19:1–13.
42. Cancès M.T., Mennucci B., Tomasi J. (1997) A new integral equation formalism for the polarizable continuum model: theoretical background and applications to isotropic and anisotropic dielectrics. J Chem Phys;107:3032–3041.
43. Mennucci B., Tomasi J. (1997) Continuum solvation models: a new approach to the problem of solute's charge distribution and cavity boundaries. J Chem Phys;106:5151.
44. Mennucci B., Cancès M.T., Tomasi J. (1997) Evaluation of solvent effects in isotropic and anisotropic dielectrics and in ionic solutions with a unified integral equation method: theoretical bases, computational implementation, and numerical applications. J Phys Chem B;101:10506–10517.
45. Tomasi J., Mennucci B., Cancès M.T. (1997) The IEF version of the PCM solvation method: an overview of a new method addressed to study molecular solutes at the QM ab initio level. J Mol Struct;464:211–226.
46. Dixon H.B.F., Perham R.N. (1968) Reversible blocking of amino groups with citraconic anhydride. Biochem J;109:312–314.
47. Kluger R., Chin J. (1982) Carboxylic acid participation in amide hydrolysis. Evidence that separation of a nonbonded complex can be rate determining. J Am Chem Soc;104:2891–2897.
48. Katagi T. (1990) AM1 study of acid-catalyzed hydrolysis of maleamic (4-amino-4-oxo-2-butenoic) acids. J Comb Chem;11:1094–1100.
49. Karaman R. (2011) Analyzing the efficiency in intramolecular amide hydrolysis of Kirby's N-alkylmaleamic acids – a computational approach. Comput Theor Chem;974:133–142.
50. Burker U., Allinger N.L. (1982) Molecular Mechanics. Washington, DC, USA: American Chemical Society.
51. Kirby A.J. (2005) Effective molarities for intramolecular reactions. J Phys Org Chem;18:101–278.

Notes

[a]Gaussian 98, Revision A.7, Pittsburgh, PA: Gaussian Inc., 1998.
[b]It should be noted that DFT calculations in the presence of a mixture of acid and water are not feasible.

Supporting information

Additional Supporting Information may be found in the online version of this article:

Appendix S1. xyz Cartesian co-ordinates for the calculated GM, INT, and TS optimized structures in processes **1–15** and **ProD 1**–**4**.

Please note: Wiley-Blackwell is not responsible for the content or functionality of any supporting materials supplied by the authors. Any queries (other than missing material) should be directed to the corresponding author for the article.